Journal of Thermal Science Vol.28, No.5 (2019) 1024−1034

https://doi.org/10.1007/s11630-019-1164-y **Article ID: 1003-2169(2019)05-1024-11**

Numerical Simulation and Optimization of Staged Combustion and NO_x Release Characteristics in Precalciner

WANG Weishu, LIAO Yihan, LIU Jun*, HUANG Zhihao, TIAN Miao

Thermal Engineering Research Centre, North China University of Water Resources and Electric Power, Zhengzhou 450011, China

Abstract: In order to study the combustion characteristics in a precalciner, the temperature and composition field in a typical Trinal-sprayed calciner were numerically analysed. The results obtained by simulation were compared to actual measurements and the simulated results were in good agreement with the measured ones. The results indicated that the aerodynamic flow field in the precalciner is satisfactory, and a symmetrical reflux occurs in the shrinkage zone of the precalciner because of air staging, which can increase the residence time of the solid particles. The temperature distribution in the furnace is uniform, and the average temperature is greater than 1200 K, which can satisfy the conditions for the pulverised coal combustion and raw material decomposition. The mass fraction distribution of oxygen, carbon monoxide, and carbon dioxide in the precalciner is closely related to the temperature distribution. The concentration of nitrogen oxides (NO_x) exhibits a trend of increasing, decreasing and then increasing, and finally tending to a stable level. Within a certain velocity range, the average temperature in the precalciner and the decomposition efficiency of the raw material increase as the flue gas velocity increases. When the flue gas velocity is 24 m/s, the overall performance of the precalciner is optimal.

Keywords: TTF precalciner, staged combustion, NO_x emission characteristics, optimization

1. Introduction

Existing studies have indicated that coal-based fuel combustion pollution from cement kilns is the third largest source of nitrogen oxides (NO_x) emissions [1]. With the increasingly critical issue of environmental protection, cement NO_x emissions, which are primarily from the combustion of fossil fuels required to heat the kiln and the chemical reaction of raw materials in the pyro-processing phase, are attracting increasing attention [2]. Staged combustion is an important technology that can effectively control the NO_x release of coal-fired boilers, improve the furnace structure, and optimise the parameters to achieve high-efficiency and low-nitrogen staged combustion of cement furnace kilns, effectively reducing pollutant emissions from cement kilns [3-5].

A number of studies have been conducted regarding precalciners. A mathematical model was used for the novel greenhouse calcium cycle process [6-7], determined the dynamics and design parameters of the precalciner, and optimised the combustion system of the precalciner, all of which can aid the design of a precalciner. However, the flow field distribution and NO_x emission characteristics in the precalciner were not considered, and it was impossible to determine the performance of the precalciner. Based on the known

Received: Feb 18, 2019 AE: YANG Bin Corresponding author: LIU Jun E-mail: ljbaihe@163.com

mathematical physics model, computational fluid dynamics (CFD) software was used to numerically simulate the effects of additives on the combustion characteristics and pollutant emission characteristics of the mixed fuel in the precalciner [8-10], and the coupled combustion mechanism of fuel combustion and raw material decomposition were obtained. However, the numerical simulation results were not reliable because of the lack of experimental results. In order to provide more accurate and reliable results, a number of scholars [11-15] experimentally studied the emission characteristics of gases, such as SO_2, CO, CO_2, and NO_x, in the pulverised coal combustion process in high-temperature cement precalcining kilns, and obtained the emission characteristics of CO_2 and other greenhouse gases and the influence of different coal types on NO_x. A number of experiments were used to study the pollutant emission characteristics of the cement production industry, and the influence of $CaCO_3$ and different coal types on the low NO_x technology of cement kilns were obtained experimentally [16-19]. However, because of the significant research and developmental costs, and extended experimental method research periods, the flow fields in the precalciner and the reaction mechanisms are difficult to determine by this method. However, numerical methods have proved to be beneficial to reveal the flow field distribution and are now widely used to study the physical and chemical mechanisms and pollutant emissions in precalciners. The *k*-ε turbulence model, Lagrange approach, and non-premixed combustion model were used to calculate turbulent flow structure, the trajectories of single particles, and fuel combustion, respectively [20-22]. In order to obtain the law of NO_x formation in different coal types, CFD software was used to analyse the influence mechanism of reburning zone conditions, CaO and different gas compositions on NO_x reduction by selective non-catalytic reduction [23-25,27]. However, the above studies are insufficient for the newer Trinal-sprayed calciner (TTF) precalciner. Compared with the older precalciner, the newer TTF precalciners have simple structure, strong adaptability to fuel, three-sprayed effect, and strong turbulent recirculation, and the feeding modes of pulverised coal and raw material have changed. These distinctive characteristics make the combustion characteristics in the newer TTF precalciner different from the older precalciner. In this study, to reduce NO_x emission and provide theoretical guidance for the actual operation of the cement industry precalciner, CFD software was used to numerically study the coupling process of the pulverised coal combustion and raw material decomposition in the typical three-sprayed TTF precalciner. The numerical results were compared with actual results, and the temperature of the furnace, the decomposition efficiency of the raw material, and the NO_x release law under different flue gas velocities were analysed. The simulation study of combustion characteristics and NO_x generation in the furnace is of great significance to optimise the furnace design, to realise energy saving and emission reduction, and to guide the safe operation of the precalciner.

2. Mathematical Modelling of Numerical Simulation and NO_x Formation

2.1 Mechanism of volatilization reaction

Devolatilization can be modelled by one or more reaction steps using the generic Arrhenius multiphase reactions capability, although normally the process is represented by one or two reaction steps. The simpler model is the single reaction model of Badzioch and Hawksley [28]. If, at time t, the coal particle consists of mass fractions C_O of raw (that is, unreacted) coal, C_{ch} of residual char, and C_A of ash, then the rate of conversion of the raw coal is:

$$\frac{dC_O}{dt} = -k_V C_O \tag{1}$$

and the rate of production of volatiles in the gas phase is given by:

$$\frac{dV}{dt} = Yk_V C_O \tag{2}$$

where Y is the actual yield of volatiles (that is, the proximate yield multiplied by a factor to correct for the enhancement of yield due to rapid heating), so that the rate of char formation is:

$$\frac{dC_{ch}}{dt} = (1-Y)k_V C_O \tag{3}$$

The rate constant k_V is expressed in Arrhenius form as:

$$k_V = A_V \exp\left(-\frac{E_V}{RT_P}\right) \tag{4}$$

where T_P is the temperature of coal particles (assumed uniform); R is the gas constant, and A_V and E_V are constants determined experimentally for the particular coal.

2.2 Mechanism of decomposition of the raw material

When you choose to solve conservation equations for chemical species, ANSYS Fluent predicts the local mass fraction of each species, Y_i, through the solution of a convection-diffusion equation for the i^{th} species. This conservation equation takes the following general form:

$$\frac{\partial}{\partial t}(\rho Y_i) + \nabla \cdot (\rho \vec{v} Y_i) = -\nabla \vec{J_i} + R_i + S_i \tag{5}$$

where R_i is the net rate of production of species i by chemical reaction (described later in this section) and S_i is the rate of creation by addition from the dispersed

phase plus any user-defined sources. An equation of this form will be solved for N-1 species where N is the total number of fluid phase chemical species presented in the system. Since the mass fraction of the species must sum to unity, the N^{th} mass fraction is determined as one minus the sum of the N-1 solved mass fractions. To minimize numerical error, the N^{th} species should be selected as that species with the overall largest mass fraction, such as N_2 when the oxidizer is air.

In this paper, there are three main chemical reactions considered in the precalciner. The formula is as follows:

$$\begin{aligned} &\text{Volatile} \rightarrow \text{CO}+\text{H}_2\text{O}+\text{N}_2 \\ &\text{CO}+\text{O}_2 \rightarrow \text{CO}_2 \\ &\text{CaCO}_3 \rightarrow \text{CO}_2+\text{CaO} \end{aligned} \tag{6}$$

2.3 Mechanism of NO_x formation

The NO_x produced by the combustion of pulverised coal in the furnace primarily include NO, NO_2, and N_2O, in which NO accounts for approximately 90% [1,25-26], and the generated NO_x is primarily thermal NO_x, prompt NO_x and fuel NO_x.

Thermal NO_x is generated when N_2 in the air is oxidised by high temperatures. The generation of thermal NO_x is related to chemical reaction kinetics and intermediate processes.

The Zeldovich NO formation rate equation is as follows [29]:

$$\frac{\mathrm{d}c_{\mathrm{NO}}}{\mathrm{d}t} = 3\times10^{14} c_{\mathrm{N_2}} c_{\mathrm{O_2}}^{1/2} \exp\left(-\frac{542000}{RT}\right) \tag{7}$$

where c_{NO}, $c_{\mathrm{N_2}}$, and $c_{\mathrm{O_2}}$ are the concentrations of NO, N_2, and O_2, respectively, T and R are the thermodynamic temperature and the molar gas constant, respectively, and t is time.

It can be seen from Eq. (7) that the primary influencing factors of thermal NO_x formation are furnace temperature and oxygen content, in which temperature is the dominant factor. Fig. 1 shows the relationship between thermal NO_x formation and temperature. When the temperature is less than 1800 K, the amount of thermal NO_x generated is small, and when the temperature is greater than 1800 K, the thermal NO_x generated increases sharply.

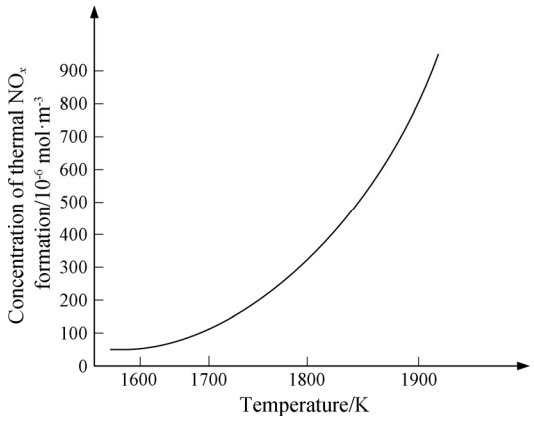

Fig. 1 Thermal NO_x formation vs temperature

Prompt NO_x is formed by the reaction of CH radicals, which are generated by the combustion of hydrocarbon fuels with N_2 in the air. It was discovered and named by Fenimore in 1971 [30].

When hydrocarbons start burning, specifically under fuel-rich conditions, a large number of CH, CH_2, CH_3, and C_2 plasma groups are decomposed, which destroy the bonds of N_2 molecules in the combustion air and react to form HCN, and CN, amongst others. The formation processes are as follows:

$$\begin{aligned} &\text{CH}+\text{N}_2 \leftrightarrow \text{HCN}+\text{N} \\ &\text{CH}_2+\text{N}_2 \leftrightarrow \text{HCN}+\text{NH} \\ &\text{C}_2+\text{N}_2 \leftrightarrow 2\text{CN} \\ &\text{HCN}+\text{OH} \leftrightarrow \text{CN}+\text{H}_2\text{O} \end{aligned} \tag{8}$$

It has been found experimentally that [13-14,23], as the combustion temperature increases, HCN first appears, reaches the highest point at the flame surface, and then decreases behind the flame surface. As the HCN concentration decreases, the amount of NO generated increases abruptly. It was also found that a significant amount of NH_i appeared when the HCN concentration began to decrease after reaching the highest point, and these amine compounds were further oxidised to form NO. Of these, HCN is an important intermediate product, and 90% of the prompt NO_x is produced by HCN. The amount of rapid NO_x formation is not affected by temperature, but is proportional to the square root of pressure.

Fuel NO_x is formed by the oxidation of nitrogenous compounds in fuel during pulverised coal combustion, and accounts for approximately 75% of the total NO_x production, in which fuel NO_x from volatiles accounts for approximately 70%, which is the primary source of NO_x formation [23-24]. The relationship of the fuel nitrogen balance in the combustion process is shown in Fig. 2.

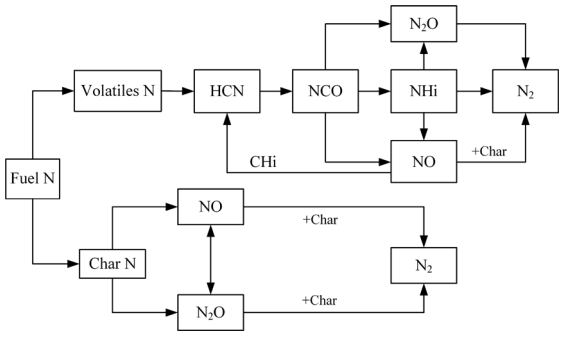

Fig. 2 Relationship of coal fuel nitrogen balance

There is volatile N and char N in the fuel, and volatile N produces intermediate HCN and NH_3, which are then continuously oxidised to form NO_x. Unoxidised HCN and NH_3 will react with NO_x to form N_2. Char N is oxidised to NO_x as the fuel is burned and, at the same time, some of the NO_x is reduced to N_2 because of the reductive nature of char. Therefore, the primary measure to reduce fuel NO_x is to control the release of volatile N in the fuel.

3. Model and Calculation Method

3.1 Physical model

The simulated object is a three-sprayed TTF precalciner of 5000 tons per day. The physical model is established according to the actual size of 1:1. The height of the precalciner is 46 m, and the diameter of the column is 7.6 m. There are four raw material inlets, two of which are in the upper part and two in the lower part, three tertiary air inlets, one of which is located in the upper part of the precalciner, and the other two in the lower part; and four coal injection pipes, which are located in the lower part of the precalciner and are between the tertiary air and the raw material inlets. There is an outlet in the upper part and an exhaust gas inlet in the lower part of the precalciner. The precalciner is shown in Fig. 3.

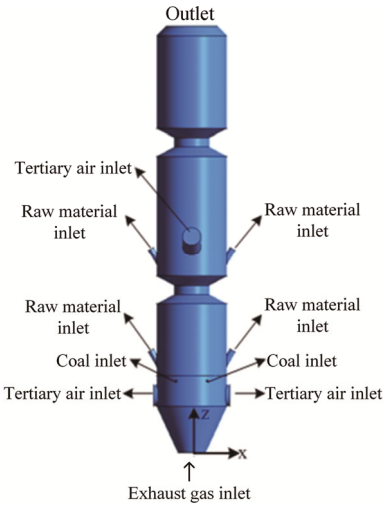

Fig. 3 Geometric model structure of precalciner

The essence of CFD is the discrete of points and regions on the specified region of the governing equation, which translates into algebraic equations defined on each grid point or region, and then solved algebraic equations iteratively [31]. Therefore, for CFD simulation, grid generation is very important. In this paper, the pulverised coal tube, raw material tube, and tertiary air tube were divided into hexahedral meshes. According to the structural characteristics of the precalciner, the precalciner was divided into four parts: upper, middle, lower and bottom. The upper part adopts structured mesh. Structured meshes can easily handle boundary conditions with high computational accuracy, and the use of structured meshes can greatly reduce the number of meshes. The middle and lower parts were unstructured meshes. The unstructured meshes are suitable for complex areas, and its node distribution is random, which can well capture the characteristics of the flow field and improve the calculation accuracy of complex areas. And the bottom was divided by regular hexahedral mesh. In order to simulate the pulverised coal combustion process and the raw material decomposition chemical reaction more accurately in the combustion zone, local mesh encryption was performed on the region with strong turbulence. After verification by the grid, the optimal number of grids was determined to be 1.25 million.

3.2 Numerical calculation method

In order to ensure the accuracy of the mathematical models which were established, some assumptions must be made about the precalciner:

(a) The fluid in the precalciner is regarded as an incompressible fluid;

(b) All the walls of the precalciner are ideal insulators, that is, the wall temperature is constant;

(c) The chemical reaction process is simplified, the main reactions are retained. Other side reactions are ignored.

The chemical reactions occurring in the precalciner are complex, including pulverised coal combustion and raw material decomposition, accompanied by strong swirling and pulsating turbulent flow. Therefore, the re-normalisation group k-ε double equation model was used to simulate the gas phase flow; the discrete phase model was used to compute the gas-solid two-phase flow, and the pulverised coal particles were set as discrete items. The two-step competitive reaction model was used to simulate the precipitation of volatiles in the pulverised coal combustion process, and the kinetic/diffusion control reaction rate model was used to simulate the coke combustion reaction related to the diffusion rate. The P-1 radiation model was used to calculate the radiation heat transfer between the gas and the particles in the precalciner. The species transport model was used to set the material properties and chemical reaction parameters to simulate the chemical reaction of the pulverised coal combustion coupled raw material decomposition, and the nitrogen oxide (NO_x and N_2O) was predicted by the "post-treatment" method. On the basis of stable combustion, using empirical formulas, the NO is primarily considered.

3.3 Boundary conditions

The correct boundary conditions and a reasonable

numerical method in the CFD software play a critical role in the accuracy of the numerical simulation results. The specific input data are as follows. The exhaust gas in the lower part of the precalciner adopts the inlet velocity, the wind speed is 27 m/s, the temperature is 1400 K, and the composition of the exhaust gas is simplified to volume fractions of 4.1% O_2, 15.4% CO_2, 0.2% CO, and 80.3% N_2. The tertiary air speed in the upper part of the precalciner is 26 m/s at a temperature of 1300 K, and the tertiary air speed in the lower part of the precalciner is 26 m/s at a temperature of 1200 K. The pulverised coal inlet adopts an inlet velocity of 40.2 m/s at a temperature of 343 K. The raw material is set as fluid, the raw material inlet adopts the mass flow inlet boundary condition, and the upper and lower part mass flow of the precalciner are both set at 25 kg/s at a temperature of 1200 K. The entire precalciner is in an environment with a local gravity acceleration of 9.8 m/s^2. The outlet pressure is −1200 Pa. The wall boundary condition uses a standard wall no slip function, and all wall temperatures are set to 1000 K except for the inlet and outlet. The method of fitting the particle size of the pulverised coal is the Rosin-Rammler distribution, and the physical properties, such as the density and diameter of the pulverised coal, are presented in Table 1. The proximate and ultimate analyses of the pulverised coal are presented in Table 2.

Table 1 Physical properties of coal particles

Particle type	Total mass flow/ $kg \cdot s^{-1}$	Density/ $kg \cdot m^{-3}$	Size distribution of coal particle/μm		
			Minimum particle size	Maximum particle size	Average particle size
Coal	6.4	1400	50	90	60

Table 2 Analysis data of pulverised coal (ar)

Proximate analysis/wt%				Ultimate analysis/wt%					
Moisture	Volatile matters	Fixed carbon	Ash	Carbon (C)	Hydro (H)	Oxygen (O)	Nitrogen (N)	Surfer (S)	Lower heating value/ $MJ \cdot kg^{-1}$
8.8	13.51	52.71	13.51	52.96	3.03	8.99	0.58	0.66	20.23

Note: ar means as-received basis.

4. Results and Discussion

4.1 Model verification

Table 3 presents the comparison between the measured data and the numerical calculation data. The measured data is from actual measurements during field operation from Sinoma cement Co., Ltd. in China. The position of the measuring point is 0.3 m, 0.6 m, and 0.9 m from the outlet of the precalciner. It can be seen that the temperature error of the three measuring points is less than 5%, within the allowable range of the project. Taking into account the diversity of the gas composition entering the furnace, the complexity of the chemical reaction of pulverised coal combustion and calcium carbonate decomposition, and the thermal insulation of the precalciner in the actual project, as well as the error of the numerical simulation calculation itself, the NO_x concentration error is also within an acceptable range, and verified the feasibility of the numerical simulation. By comparison, it can be seen that the CFD numerical method can simulate the process of pulverised coal combustion and decomposition of raw material in the precalciner and predict the NO_x concentration at the outlet of the precalciner. Due to the complexity and difficulty of the experiment, numerical simulation is now used to study the flow field distribution in the precalciner and optimize the operating parameters of the precalciner.

Table 3 Comparisons between simulation and measurements

	Temperature/K			Average NO_x concentration of precalciner /$mg \cdot N^{-1} \cdot m^{-3}$
	0.3 m	0.6 m	0.9 m	
Calculated data	1013.6	1009.9	1007.5	617.7
Measured data	981	1020	1053	670
Error/%	3.32	1	4.32	7.8

4.2 Analysis of velocity distribution

The distribution of aerodynamic flow in the furnace is a primary influencing factor for stable combustion in the furnace. A good flow field in the furnace increases the residence time of pulverised coal and is beneficial to the burning of pulverised coal. Therefore, it is essential to study the velocity field distribution of the precalciner. Fig. 4(a) and 4(b) are the vector diagrams of the X=0 and Y=0 section, respectively. It can be seen that the aerodynamic flow of the precalciner is well distributed and the velocity distribution is regular. There are symmetrical reflux zones in the bottom cone portion and the central cylindrical portion of the precalciner. In the bottom cone portion, because of the high-speed exhaust gas injection, the tertiary air is squeezed to the sides to form a pressure difference. Because of this pressure difference, part of the air flow direction is downwards, and two symmetrical

reflux areas are formed at the bottom of the precalciner, which is not only beneficial to the round-trip of materials and residence time of pulverised coal particles but also beneficial for increasing the mixing of pulverised coal and $CaCO_3$. Finally, the combustion of pulverised coal and the decomposition of $CaCO_3$ are guaranteed. In the central cylindrical part, the velocity of the airflow increases sharply after passing through the lower portion, forming a spraying shape. Because of the mixing of the upper tertiary air, a large reflux zone in the middle of the precalciner is formed, exhibiting a spurt effect, which is in accordance with the distribution of the aerodynamic flow field in the precalciner.

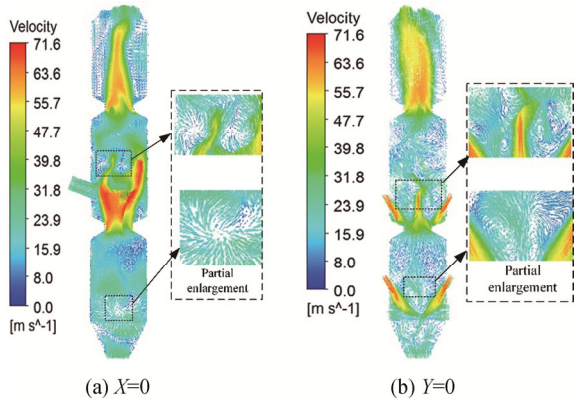

(a) X=0 (b) Y=0

Fig. 4 Speed vectors in the different sections of precalciner

4.3 Analysis of temperature distribution

The temperature field distributions of the X=0 and Y=0 sections in the precalciner are shown in Fig. 5(a) and 5(b), respectively. It can be seen that the temperature distribution across the whole furnace is uniform, with the highest furnace temperature in the lower tertiary air and pulverised coal area, and the lower tertiary air area is the primary combustion area. In the lower cylinder area of the precalciner, the temperature in the primary combustion zone of the X-section is high on both sides and low in the centre of the furnace, and the temperature decreases in the direction of the centre of the furnace. The temperature in the primary combustion zone can reach 1500–2200 K, which can satisfy the temperature requirements of raw material decomposition. The high-temperature flue gas from the kiln tail and the high-temperature tertiary air are mixed in the lower cylinder. The pulverised coal is injected from the coal injection pipe into the furnace, and the volatile matter is burned here to form a primary combustion zone, where the chemical reaction of the raw material decomposition, which could absorb a significant amount of heat, also occurs. As can be seen from Fig. 4, because of the introduction of the upper tertiary air, reflux occurs in the area below the cylinder in the middle of the precalciner, prolonging the residence time of the coal powder and the raw material, and the unburned coke continues to burn. Therefore, stable ignition and full combustion of the pulverised coal particles are ensured.

The temperature field distribution of different sections along the height of the furnace is shown in Fig. 6. It can be seen that along the entire height of the precalciner, the temperature generally increases and then decreases, and then increases and decreases again. The temperature finally reaches a stable state above the central cylinder at the exit of the furnace. It can be seen that the high-temperature kiln flue gas enters the precalciner and, because of the temperature difference, the temperature is instantaneously decreased. Because of the rapid combustion of pulverised coal and devolatilization, the temperature close to the pulverised coal nozzle is significantly increased. As can be seen from Fig. 5, the maximum temperature in the furnace can reach 2300 K. The temperature is then decreased because of the absorption of heat by the decomposition of the raw material. The unburned pulverised coal particles continue to burn because of the addition of the upper tertiary airflow in the area of the third duct on the cylinder in the middle of

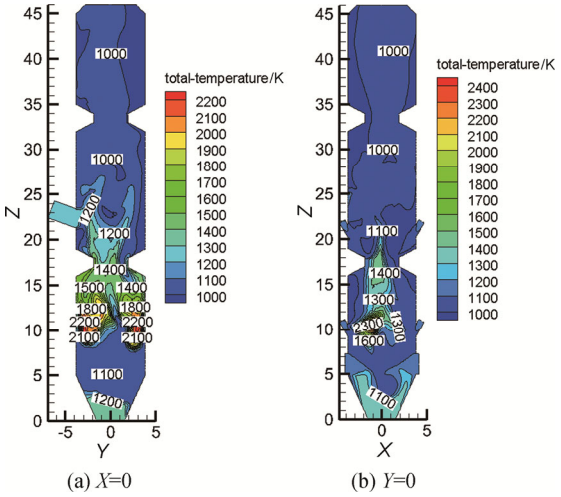

(a) X=0 (b) Y=0

Fig. 5 Temperature distribution on centre longitudinal cross section of precalciner

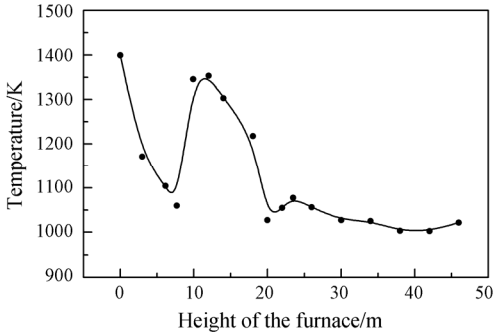

Fig. 6 Average temperature profile of section along height of precalciner

the precalciner and, accompanied by the decomposition of the raw material, the temperature in the furnace increases marginally. The flue gas finally enters the upper cylinder, and the temperature gradually decreases and stabilises.

4.4 Analysis of composition distribution

Figs. 7-9 show the mass fraction distribution of oxygen, CO, and CO_2 of the longitudinal section X=0 and Y=0 in the centre of the precalciner, respectively. Combined with the analysis in Fig. 5, the mass fraction distribution of oxygen, CO, and CO_2 is related to temperature. There are relatively low oxygen mass fractions and higher mass fraction of CO and CO_2 in the higher temperature regions in the precalciner. Conversely, at lower temperatures, the mass fraction of oxygen is relatively high and the mass fractions of CO and CO_2 are relatively low. It can be seen from Fig. 7 that the mass fraction of oxygen is the greatest at the lower two tertiary air inlets, followed by the upper air inlet. The oxygen is gradually consumed with the combustion of the pulverised coal, and the mass fraction of oxygen is gradually decreased along the height of the furnace. The mass fraction distribution trend of oxygen is greater in the middle and lower on both sides of the furnace along the height of the furnace at the lower cylinder of the X=0 section, which is opposite to the distribution trend of the temperature which is lower in the middle and higher on both sides of the furnace at the lower cylinder in Fig. 5. The precalciner uses the method of grading air distribution. The pulverised coal is incompletely combusted in the lower part of the precalciner to form CO. The largest mass fraction of CO exists at the entrance of the pulverised coal, which exhibits a high concentration on both sides and low concentration in the middle of the furnace at the lower cylinder of the X=0 section. The mass fraction of CO gradually decreases as the height of the furnace increases, and the mass fraction of CO is stabilised in the upper part of the precalciner. The mass fraction of CO_2 in the lower part of the cylinder in the X=0 section exhibits a high concentration on both sides and a low concentration in the middle of the furnace. The mass fraction of CO_2 tends to be stable in the upper part of cylinder, which has the same distribution trend as that of the temperature. In the combustion area, pulverised coal is burned to produce a large amount of CO because the amount of oxygen is deficient in the initial combustion stage. With the injection of the upper inlet air in the upper part of the furnace, the CO reacts with the excess oxygen to form CO_2, and the mass fraction of CO gradually decreases to approximately zero at the exit of the decomposition furnace. The high temperature in the combustion zone is suitable for the chemical reaction of $CaCO_3$ to generate a significant

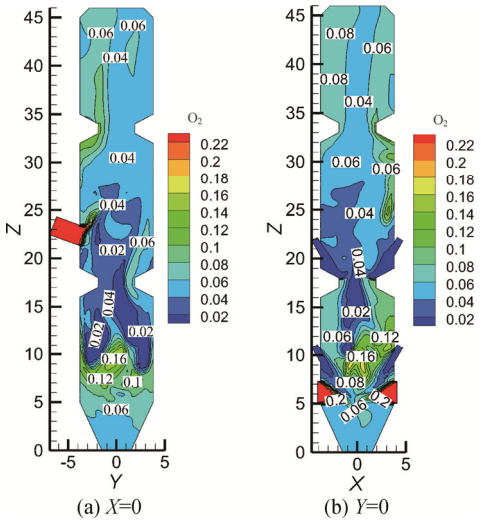

Fig. 7 Mass fraction of oxygen in centre section of precalciner

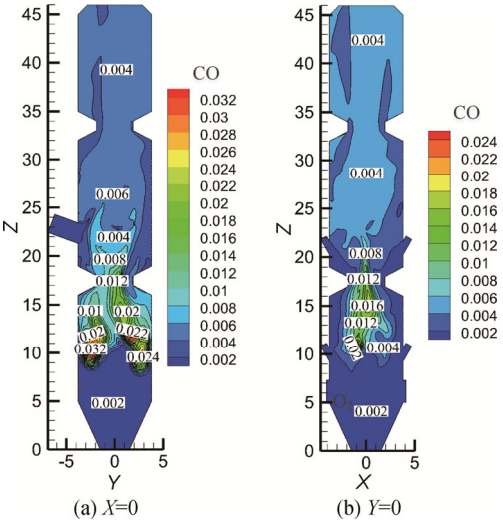

Fig. 8 Mass fraction of CO in centre section of precalciner

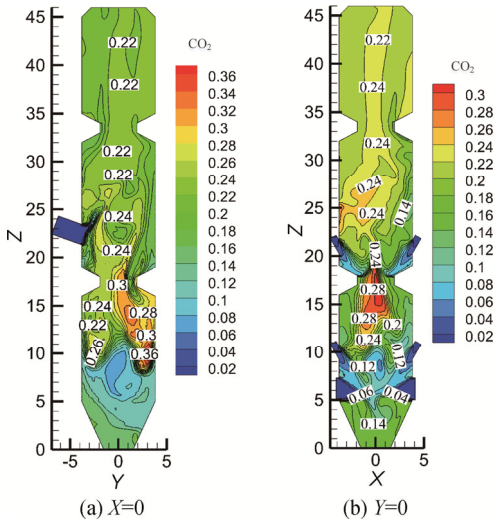

Fig. 9 Mass fraction of CO_2 in centre section of precalciner

amount of CaO and CO_2. Therefore, there is a large amount of CO_2 in the lower cylinder region, and the mass fraction of CO_2 tends to be stable above the upper air inlet.

Figs. 10-11 show the mass fraction distribution of $CaCO_3$ and CaO in each section along the height of the furnace, respectively. It can be seen that, in the lower cylinder of the precalciner, the mass fraction of $CaCO_3$ is the greatest at the inlet of the raw material at Z=10 m. As the height of the furnace increases, $CaCO_3$ absorbs heat, and starts to decompose to form CaO, the mass fraction of $CaCO_3$ decreases, and the mass fraction of CaO increases. At approximately Z=14 m, the mass fraction of $CaCO_3$ gradually increases because of the feed of the raw material tube. The mass fraction of $CaCO_3$ reaches a second peak at Z=21 m in the upper raw material inlet, and then continues to decompose and form CaO. The mass fraction of $CaCO_3$ continues to decrease, the mass fraction of CaO continues to increase, and the mass fractions of $CaCO_3$ and CaO in the upper part of the decomposition furnace tend to be stable. It can also be seen from Fig. 11 that the mass fraction of CaO in the lower part of the decomposition furnace increases rapidly. This is because the pulverised coal in this area is burned vigorously, and the temperature in the furnace is the highest, resulting in the highest decomposition rate of $CaCO_3$ and the greatest CaO formation rate.

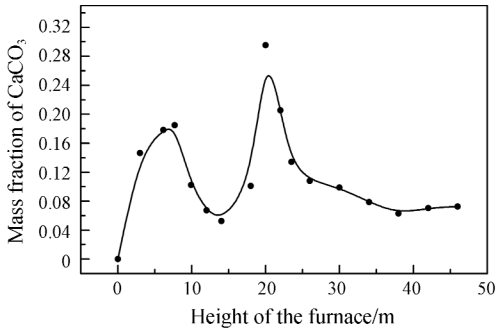

Fig. 10 Mass fraction distribution of $CaCO_3$ along height of precalciner

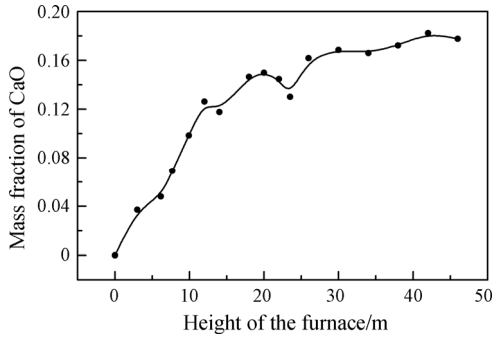

Fig. 11 Mass fraction distribution of CaO along height of precalciner

4.5 Analysis of NO_x distribution law

Fig. 12(a) and 12(b) show the concentration distribution of NO_x (the unit is mg/(N·m^3)) on the X=0 and Y=0 sections of the centre longitudinal section of the furnace, respectively. It can be seen that the high concentration region of NO_x is primarily distributed in the vicinity of the combustion zone of the lower cylindrical part of the precalciner and the tertiary air duct in the middle cylinder of the precalciner. The concentration of NO_x in the upper part of the precalciner gradually becomes stable. Combined with the temperature field distribution of the precalciner of Fig. 5, it is known that the region with a high NO_x concentration corresponds to the primary combustion zone where the temperature of the precalciner is relatively high, the pulverised coal is vigorously burned in this region, the temperature reaches 2200 K, and fuel NO_x and thermal NO_x are generated at the same time. Although the oxygen content in the cylinder of the middle of the precalciner is relatively high, the temperature in this region is lower than that in the lower cylinder, the increase in NO_x is insignificant, and less NO_x is generated at the outlet of the furnace. Therefore, NO_x formation is highly dependent on the temperature and mass fraction of oxygen. Reasonable temperatures and oxygen concentrations help to suppress NO_x formation.

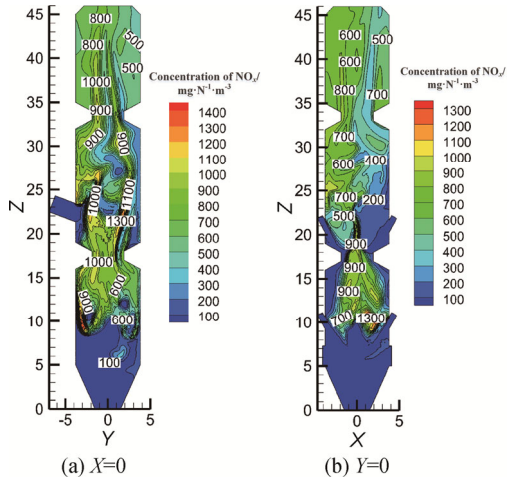

(a) X=0 (b) Y=0

Fig. 12 Concentration of NO_x on centre longitudinal cross section of precalciner

Fig. 13 shows the concentration distribution of NO_x in the height direction of the precalciner (Z-axis) (the unit is mg/(N·m^3)). It can be seen that, as the height of the furnace increases, the concentration of NO_x increases rapidly, and the highest NO_x concentration occurs close to the Z=14 m section, and then decreases. At Z=20 m, the concentration of NO_x is the lowest, and then continues to increase and then remains stable. In the Z=0–14 m region, the average temperature in the precalciner is significant,

and the oxygen content is sufficient. The nitrogen compounds in the coal powder are oxidised to form NO_x, which causes the concentration of NO_x to increase sharply. In the Z=14–20 m region, the mass concentration of oxygen is insufficient, the CO generated by incomplete combustion reduces NO_x to N_2 and, at the same time, N_2 is formed by the chemical reaction between NO_x and other intermediates, such as HCN, and the concentration of NO_x decreases. In the Z=20–26 m region, because of the input of the upper tertiary air, the pulverised coal continues to burn, causing the temperature in the precalciner to increase marginally and the concentration of NO_x to increase. A "gentle" peak appears at Z=26 m, after which there is a decrease because of unburned coke and NO_x. The reaction reduces NO_x to N_2, so the concentration of NO_x decreases slightly and stabilises close to the exit of the precalciner, and the average concentration of NO_x of outlet cross-section is approximately 617.7 mg/(N·m^3).

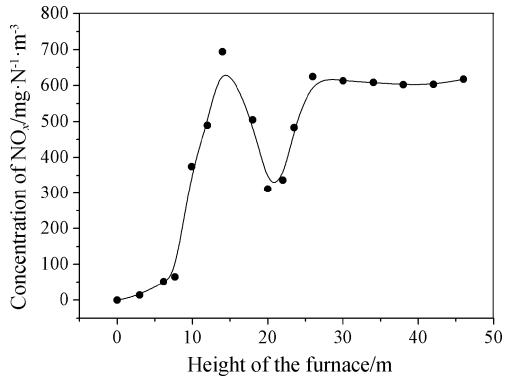

Fig. 13 Concentration distribution of NO_x along height of precalciner

Compared to other kind of precalciners, there are different characteristics of NO_x emission. The combustion characteristics in vortexing precalciner was numerically studied by Mei [10]. It can be known that tertiary air entered the swirl calciner tangentially, decomposed the raw material entering from the upper cyclone, and along the height of the vortexing precalciner, the concentration of NO_x continued to rise, because of the vortex effect, the concentration of NO_x had a fast ascending region, along the height of the precalciner, the rate of NO_x formation decreased. Huang [23] numerically analysed NO emission in a dual combustion and denitrator process precalciner (DD-PRC), and the results showed that along the height of the DD-PRC, the concentration of NO in the DD-PRC first increased, then decreased slightly, and finally came to be stable. This was because the DD-PRC had only one shrinkage compared to the TTF precalciner, without air staging and fuel staging, which led to a higher temperature and more generated thermal NO_x in the DD-PRC. There are many differences in structural and combustion characteristics in the furnace between the newer TTF precalciner and other kind of precalciners. Therefore, it is very important and necessary to study the NO_x release characteristics of the newer TTF precalciner.

5. Numerical Optimization

In order to optimise the process parameters of the precalciner, reduce NO_x emissions, and achieve energy saving and environmental protection, the staged combustion characteristics of the precalciner under typical flue gas velocity were studied. A comparison between optimised and original conditions of the average temperature, mass fraction of $CaCO_3$ and CaO, concentration distribution of NO_x in the precalciner is shown in Fig. 14. It can be seen that the pulverised coal in the precalciner can be stably burned and coupled with raw material decomposition under different flue gas velocity conditions, the temperature field, composition field, and concentration distribution trend of NO_x under each working condition are consistent. Within a certain range, with the increase in flue gas velocity, the average temperature in the precalciner increases, and the decomposition efficiency of the raw material also increases. When this range is exceeded, the average temperature in the precalciner does not increase, but decreases, and the decomposition rate of the raw material also decreases. Under the original condition (v=27 m/s), the average temperature in the precalciner is the highest, and the decomposition efficiency of $CaCO_3$ is the greatest, however, the NO_x concentration at the outlet of the precalciner reaches 617.7 mg/(N·m^3), which is greater than that under other conditions. The higher the flue gas velocity, the higher the concentration of NO_x at the outlet of the precalciner. When the flue gas velocity rises to 30 m/s, the concentration of NO_x at the outlet of the precalciner is 846.8 mg/(N·m^3), which is 37.1% higher than that when the velocity is 27 m/s, because the flue gas velocity affects the combustion in the precalciner, the higher the velocity is, the stronger the disturbance in the furnace, the more violent combustion of pulverised coal, and the more fuel NO_x is produced. On the other hand, when the flue gas velocity is too large, the raw material in the precalciner cannot be completely decomposed, and the temperature in the furnace is high, resulting in the generation of thermal NO_x. Considering the above discussions, when the flue gas velocity is v=24 m/s, the overall average temperature in the precalciner is higher, the decomposition efficiency of $CaCO_3$ is greater, and a larger amount of CaO is generated, the concentration of NO_x at the outlet of the precalciner is only 419.6 mg/(N·m^3), which is 32.07% less than the original condition.

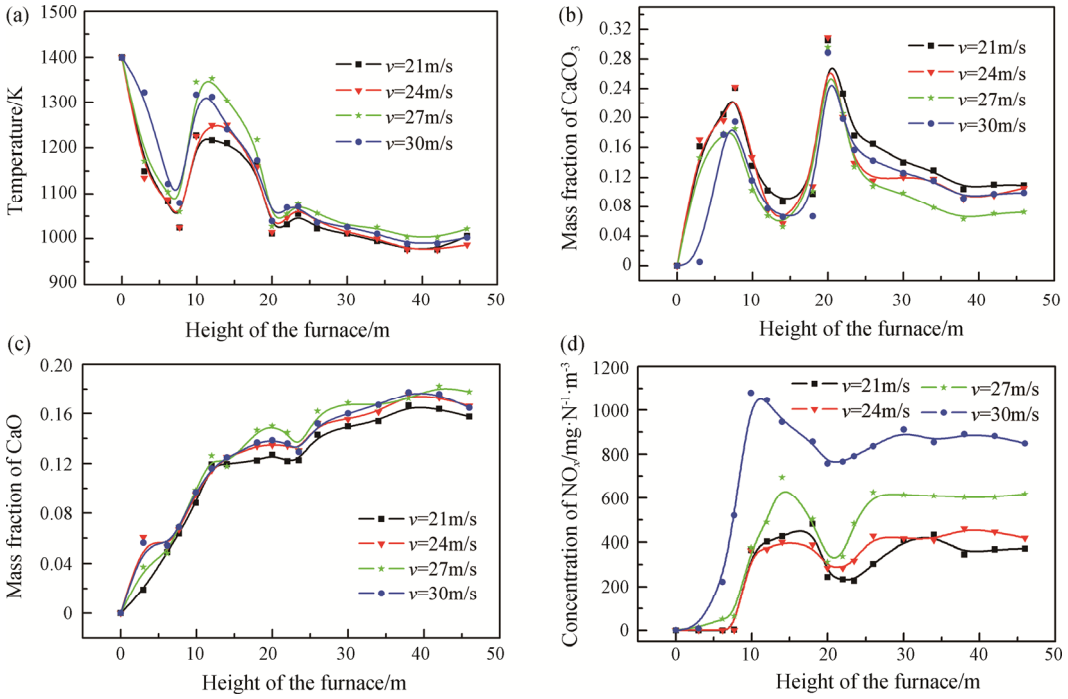

Fig. 14 Comparison of different cases: (a) average temperature; (b) mass fraction of $CaCO_3$; (c) mass fraction of CaO; and (d) NO_x concentration

6. Conclusions

A full-scale numerical simulation of the 5000-tons-per-day TTF precalciner was conducted, the combustion characteristics of air stages and raw material stages were analysed, and the velocity field, temperature field, composition field, and NO_x distribution law were numerically predicted. The numerical method was shown to be reliable by comparison of simulation data with experimental data. The results indicated that, along the height of the precalciner, the average temperature in the furnace first increases and decreases, and then increases again and gradually decreases to stable level. The mass fraction of $CaCO_3$ increases and decreases alternately, the mass fraction of CaO keeps increasing, the NO_x concentration first increases and then decreases, followed by another increase, and finally tends to be stable. In addition, this study analysed the influence of different flue gas velocities. It can be concluded that the combustion in the precalciner is stable under different flue gas velocities, and the temperature in the furnace can meet the decomposition requirements for raw materials. The temperature distribution law, composition distribution law and NO_x formation law are consistent. With increasing flue gas velocity, the average temperature of the precalciner increases and the decomposition rate of raw material increases. When the flue gas velocity increases to 30 m/s, the average temperature in the furnace does not increase, but decreases, and the decomposition rate of raw material decreases. The greater the flue gas velocity, the greater the NO_x concentration at the outlet section of the precalciner. Considering all these factors, a flue gas velocity of 24 m/s is the most suitable.

Acknowledgments

The authors are grateful for the support provided by the National Key R&D Plan (under No.2018YFB0604103) and the Elsevier Language Editing Service.

References

[1] Brian M.D., Stuart M.K., Yan C.Y., et al., Modeling ozone in the eastern U.S. using a fuel-based mobile source emissions inventory. Environmental Science and Technology, 2018, 52(13): 7360–7370.

[2] Brown D., Sadiq R., Hewage K., An overview of air emission intensities and environmental performance of grey cement manufacturing in Canada. Clean Technologies and Environmental Policy, 2014, 16(6): 1119–1131.

[3] Bai T., Sun B., Guo Y., et al., Effects of tertiary air staged combustion on NO_x emission characteristic in a pulverized-coal boiler with swirl burner. Lecture Notes in Electrical Engineering, 2012, 155: 255–263.

[4] Ma H.K., Hsieh D.M., The reduction of thermal nitrogen oxides (NO_x) emission using staged combustion in

furnace. Journal of Thermal Science, 1993, 2(1): 61–69.

[5] Keefe B.P., Shenk R.E., Staged combustion for low-NO_x calciners. Cement Industry Technical Conference. IEEE Xplore, FL, USA, 2002, pp. 255–264.

[6] Ramezani M., Tremain P., Shah K., et al., Kinetics and design parameter determination for a calciner reactor in unique conditions of a novel greenhouse calcium looping process. Energy and Fuels, 2017, 32: 33–43.

[7] Fellaou S., Harnoune A., Seghra M.A., et al., Corrigendum to "Statistical modelling and optimization of the combustion efficiency in cement Kiln precalciner". Energy, 2018, 115(15): 351–359.

[8] Lamani V.T., Yadav A.K., Narayanappa K.G., Influence of low-temperature combustion and dimethyl ether-diesel blends on performance, combustion, and emission characteristics of common rail diesel engine: a CFD study. Environmental Science and Pollution Research, 2017, 24(18): 1–10.

[9] Kong S., A study of natural gas/DME combustion in HCCI engines using CFD with detailed chemical kinetics. Fuel, 2007, 86(10–11): 1483–1489.

[10] Mei S., Xie J., Chen X., et al., Numerical simulation of the complex thermal processes in a vortexing precalciner. Applied Thermal Engineering, 2017, 125(7): 652–661.

[11] Chen X., Xie J., Mei S., et al., NO_x and SO_2 emissions during co-combustion of RDF and anthracite in the environment of precalciner. Energies, 2018, 11(2): 337–349.

[12] Jin Y., Li Y., Liu F., Combustion effects and emission characteristics of SO_2, CO, NO_x, and heavy metals during co-combustion of coal and dewatered sludge. Frontiers of Environmental Science and Engineering, 2016, 10(1): 201–210.

[13] Hashimoto N., Watanabe H., Kurose R., et al., Effect of different fuel NO models on the prediction of NO formation/ reduction characteristics in a pulverized coal combustion field. Energy, 2017, 118(1): 47–59.

[14] Shaddix C.R., Molina A., Fundamental investigation of NO_x, formation during oxy-fuel combustion of pulverized coal. Proceedings of the Combustion Institute, 2011, 33(2): 1723–1730.

[15] Mikulcic H., Berg von E., Vujanović M., et al., Numerical analysis of cement calciner fuel efficiency and pollutant emissions. Clean Technologies and Environmental Policy, 2013, 15(3): 489–499.

[16] Fu S., Qiang S., Qiang Y., Study on the catalysis of $CaCO_3$, in the SNCR deNO_x, process for cement kilns. Chemical Engineering Journal, 2015, 262: 9–17.

[17] Yoshiie R., Hikosaka N., Nunome Y., et al., Effects of flue gas re-circulation and nitrogen contents in coal on NO_x emissions under oxy-fuel coal combustion. Fuel Processing Technology, 2015, 136: 106–111.

[18] Bulysova L.A., Gorban' V.D., The effect of fuel and air agitation on the combustion process in a low-emission combustion chamber. Thermal Engineering, 2013, 60(9): 619–627.

[19] Rahman A., Rasul M.G., Khan M.M.K., et al., Recent development on the uses of alternative fuels in cement manufacturing process. Fuel, 2015, 145: 84–99.

[20] Zroychikov N.A., Kaverin A.A., Numerical study of bituminous coal combustion in a boiler furnace with bottom blowing. Thermal Engineering, 2016, 63(11): 802–812.

[21] Askarova A.S., Messerle V.E., Ustimenko A.B., et al., Numerical simulation of pulverized coal combustion in a power boiler furnace. High Temperature, 2015, 53(3): 445–452.

[22] Zheng Y., Gao X., Sheng C., Impact of co-firing lean coal on NO_x emission of a large-scale pulverized coal-fired utility boiler during partial load operation. Korean Journal of Chemical Engineering, 2017, 34(4): 1273–1280.

[23] Huang L., Lu J., Hu Z., et al., Numerical simulation and optimization of NO emissions in a precalciner. Energy and Fuels, 2006, 20(1): 164–171.

[24] Sun Y., Fan W., Zhu T., et al., Effect of CaO on NO_x reduction by selective non-catalytic reduction under variable gas compositions in a simulated cement precalciner atmosphere. International Journal of Environmental Research and Public Health, 2017, 14(12): 1474–1485.

[25] Fan W., Zhu T., Sun Y., et al., Effects of gas compositions on NO_x reduction by selective non-catalytic reduction with ammonia in a simulated cement precalciner atmosphere. Chemosphere, 2014, 113: 182–187.

[26] Boardman R.D., Eatough C.N., Germane G.J., et al., Comparison of measurements and predictions of flame structure and thermal NO_x, in a swirling, natural gas diffusion flame. Combustion Science and Technology, 1993, 93(3): 193–210.

[27] Mikulčić H., Vujanović M., Fidaros D.K., et al., The application of CFD modelling to support the reduction of CO_2, emissions in cement industry. Energy, 2012, 45(1): 464–473.

[28] Badzioch S., Hawksley P.G.W., Kinetics of thermal decomposition of pulverized coal particles. Industrial & Engineering Chemistry Process Design and Development, 1970, 9(4): 521–530.

[29] Miller R., Davis G., Lavoie G., et al., A Super-extended Zel'dovich mechanism for NO_x modeling and engine calibration. International Congress and Exposition, Michigan, USA, 1998, pp. 1–11.

[30] Fenimore C.P., Formation of nitric oxide in premixed hydrocarbon flames. Symposium on Combustion, 1971, 13: 373–380.

[31] Roache P.J., Computational fluid dynamics. Hermosa, Albuquerque, America, 1972.